

Central black hole mass in the distant tidal disruption event candidate of *Swift* J2058.4+0516

XUEGUANG ZHANG^{*1}

¹*School of Physics and technology, Nanjing Normal University, No. 1, Wenyuan Road, Nanjing, 210023, P. R. China*

ABSTRACT

In the manuscript, central black hole (BH) mass is estimated in the distant TDE (tidal disruption event) of *Swift* J2058.4+0516 as the second candidate of relativistic jet birth related to TDE. *Swift* J2058.4+0516 have quite different BH masses estimated through different indirect methods in the literature. Therefore, it is necessary and interesting to determine the central BH mass in *Swift* J2058.4+0516 by one another independent method. Here, based on the theoretical TDE model applied to describe the long-term time-dependent X-ray variabilities of *Swift* J2058.4+0516, the central BH mass can be well determined to be around $1.05_{-0.29}^{+0.39} \times 10^5 M_{\odot}$, after kind considerations of suggested intrinsic beaming effects from such relativistic jet tightly related to TDE. Moreover, the *Swift* J2058.4+0516 is an unique object in the space of BH masses versus energy transfer efficiencies of the reported TDE candidates, providing interesting clues to detect and/or anticipate candidates of relativistic TDE to make the birth of relativistic jets.

Keywords: galaxies:active - galaxies:nuclei - galaxies:individual:*Swift* J2058.4+0516- transients:tidal disruption events

1. INTRODUCTION

Swift J2058.4+0516 (= *Swift* J20:58:19.90+05:13:32) has been reported as a Tidal Disruption Event (TDE) candidate in Cenko et al. (2012) by the long-term X-ray variabilities discovered by the Burst Alert Telescope (Barthelmy et al. 2005) on the *Swift* satellite (Gehrels et al. 2004), and then by the long-term X-ray variabilities discussed and reported in Pasham et al. (2015) and in Wiersema et al. (2020), and also reported as the second candidate of relativistic TDE to make the birth of relativistic jets similar as the results in *Swift* J1644+57 well discussed in Burrows et al. (2011); Zauderer et al. (2011); Berger et al. (2012); Mangano et al. (2016); Eftekhari et al. (2018). Moreover, as the shown results in Fig. 1 in Pasham et al. (2015), there are similar time-dependent optical and X-ray variability properties. Therefore, significant correlation between X-ray and optical light curves can be confirmed in *Swift* J2058.4+0516, providing further evidence to support that it is also an efficient way to detect the TDE by X-ray properties in *Swift* J2058.4+0516, although most TDEs are commonly detected and reported by optical variability properties. Among the reported more than 80 TDE candidates (Komossa & Bade 1999; Komossa et al. 2004; van Velzen et al. 2011;

Gezari et al. 2012; Merloni et al. 2015; Holoien et al. 2016; Liu et al. 2017; Wyrzykowski et al. 2017; Wang et al. 2018; Gromadzki et al. 2019; van Velzen et al. 2019; Wevers et al. 2019; Anderson et al. 2020; Hinkle et al. 2021) (see detail in <https://tde.space>) with a star tidally disrupted by central massive black hole (BH) leading to time-dependent structure evolutions of accreting flows around the central BH, *Swift* J2058.4+0516 is the target in the manuscript, in order to find more clues on properties of central BH mass of *Swift* J2058.4+0516, mainly because of the inconsistent BH masses of *Swift* J2058.4+0516 reported in the literature.

In the literature, there are quite different reported BH masses in *Swift* J2058.4+0516. Cenko et al. (2012) have discussed that the central BH mass of *Swift* J2058.4+0516 should be smaller than $10^8 M_{\odot}$ after considerations of the shortest X-ray variability time scale in *Swift* J2058.4+0516 and considerations of the BH fundamental plane discussed in Gultekin et al. (2009). Pasham et al. (2015) have reported the central BH mass in *Swift* J2058.4+0516 to be in the range from $10^4 M_{\odot}$ to $10^6 M_{\odot}$, after analyzing properties of the sudden decline with proposed transition from super-Eddington to sub-Eddington accretion in *Swift* J2058.4+0516. Meanwhile, if a white dwarf rather than a main-sequence star was tidally disrupted in central region of *Swift* J2058.4+0516 as discussed in Krolik & Piran (2011) for *Swift* J1644+57, the central BH mass could be smaller than $10^5 M_{\odot}$ in *Swift* J2058.4+0516. More recently, after considerations of X-ray spectral properties, Seifina et al. (2017) have shown that the central BH

mass of *Swift* J2058.4+0516 should be larger than $2 \times 10^7 M_\odot$ with redshift $z = 1.1853$ accepted, through the scaling technique (Shaposhnikov & Titarchuk 2009; Titarchuk & Seifina 2017) applied with the Galactic BHs, GRO J1655-40, GX 339-4, Cyg X-1 and 4U 1543-47 as reference sources. It is clear that different techniques/methods with different considerations lead to very different central BH masses of *Swift* J2058.4+0516. Once, there was a more robust technique applied to determine the accurate central BH mass of *Swift* J2058.4+0516, central engine could be clearer enough in *Swift* J2058.4+0516. Therefore, it is important and interesting to determine the central BH mass in the TDE of *Swift* J2058.4+0516 through one another independent method.

Commonly, there are some convenient methods/techniques applied to measure/estimate BH masses of AGN and/or quiescent galaxies, such as the well-known $M_{\text{BH}} - \sigma$ relation (Ferrarese & Merritt 2000; Gebhardt et al. 2000; Kormendy & Ho 2013; Savorgnan & Graham 2015) and the well-applied Virialization method (Peterson et al. 2004; Shen et al. 2010; Rafiee & Hall 2011). More recently, TDEs properties can be well applied to determine central BH masses, such as the results shown and discussed in Guillochon et al. (2014); Mockler et al. (2019); Zhou et al. (2021), etc. Due to weak host galaxy spectroscopic absorption features and lack of broad emission lines, neither the $M_{\text{BH}} - \sigma$ relation nor the Virialization method can be applied to measure/estimate the central BH mass in *Swift* J2058.4+0516. However, to accept a TDE with a central main-sequence star tidally disrupted to describe the observed long-term X-ray variabilities in *Swift* J2058.4+0516, the central BH mass of *Swift* J2058.4+0516 can be well determined, which is the main objective of the manuscript. Section 2 presents the methods and model to describe X-ray variabilities of *Swift* J2058.4+0516 by the theoretical TDE model. Section 3 gives our main results and necessary discussions. Section 4 gives our summaries and conclusion. In the manuscript, we have adopted the cosmological parameters $H_0 = 70 \text{ km} \cdot \text{s}^{-1} \text{ Mpc}^{-1}$, $\Omega_\Lambda = 0.7$ and $\Omega_m = 0.3$.

2. METHODS AND MODEL

In order to well describe the X-ray variabilities of *Swift* J2058.4+0516 by the theoretical TDE model, the following five steps are applied.

First, standard templates of viscous-delayed accretion rates in TDEs are created. Based on the discussed dM/dE provided in (Guillochon et al. 2014, 2018; Mockler et al. 2019), templates of fallback material rate

$$\dot{M}_{fbt} = dM/dE \times dE/dt \quad (1)$$

can be created for the standard cases with central BH mass $M_{\text{BH}} = 10^6 M_\odot$ and disrupted main-sequence star of $M_* = 1 M_\odot$ and with a grid of the listed impact parameters β_t in

Guillochon & Ramirez-Ruiz (2013) with dE/dT calculated by

$$dE/dt = \frac{(2 \pi G M_{\text{BH}})^{2/3}}{3 t^{5/3}} \quad (2)$$

. Then, considering the viscous delay as discussed in Guillochon & Ramirez-Ruiz (2013); Mockler et al. (2019) by the viscous timescale T_{vis} , templates of viscous-delayed accretion rates \dot{M}_{at} can be determined by

$$\dot{M}_{at} = \frac{\exp(-t/T_{\text{vis}})}{T_{\text{vis}}} \int_0^t \exp(t'/T_{\text{vis}}) \dot{M}_{fbt} dt' \quad (3)$$

. And a grid of 31 $\log(T_{\text{vis}, t}/\text{years})$ range from -3 to 0 are applied to create templates \dot{M}_{at} for each impact parameter. The final templates of \dot{M}_{at} include 736 (640) time-dependent viscous-delayed accretion rates for 31 different T_{vis} of each 23 (20) impact parameters for the main-sequence star with polytropic index γ of 4/3 (5/3).

Second, for a TDE with model parameters of β and T_{vis} different from the list values in β_t and in $T_{\text{vis}, t}$, the actual viscous-delayed accretion rates \dot{M}_a are created by the following two linear interpolations. Assuming that β_1, β_2 in the β_t are the two values nearer to the input β , and that $T_{\text{vis}1}, T_{\text{vis}2}$ in the $T_{\text{vis}, t}$ are the two values nearer to the input T_{vis} , the first linear interpolation is applied to find the viscous-delayed accretion rates with input T_{vis} but with $\beta = \beta_1$ and $\beta = \beta_2$ by

$$\begin{aligned} \dot{M}_a(T_{\text{vis}}, \beta_1) &= \dot{M}_{at}(T_{\text{vis}1}, \beta_1) + \\ &\frac{T_{\text{vis}} - T_{\text{vis}1}}{T_{\text{vis}2} - T_{\text{vis}1}} (\dot{M}_{at}(T_{\text{vis}2}, \beta_1) - \dot{M}_{at}(T_{\text{vis}1}, \beta_1)) \\ \dot{M}_a(T_{\text{vis}}, \beta_2) &= \dot{M}_{at}(T_{\text{vis}1}, \beta_2) + \\ &\frac{T_{\text{vis}} - T_{\text{vis}1}}{T_{\text{vis}2} - T_{\text{vis}1}} (\dot{M}_{at}(T_{\text{vis}2}, \beta_2) - \dot{M}_{at}(T_{\text{vis}1}, \beta_2)) \end{aligned} \quad (4)$$

. Then, the second linear interpolation is applied to find the viscous-delayed accretion rates with input T_{vis} and with input β by

$$\begin{aligned} \dot{M}_a(T_{\text{vis}}, \beta) &= \dot{M}_a(T_{\text{vis}}, \beta_1) + \\ &\frac{\beta - \beta_1}{\beta_2 - \beta_1} (\dot{M}_a(T_{\text{vis}}, \beta_2) - \dot{M}_a(T_{\text{vis}}, \beta_1)) \end{aligned} \quad (5)$$

. Third, for a TDE with input model parameters of M_{BH} and M_* different from $10^6 M_\odot$ and $1 M_\odot$, the actual viscous-delayed accretion rates \dot{M} and the corresponding time information in observer frame are created by the following scaling relations as shown in Guillochon et al. (2014); Mockler et al. (2019),

$$\begin{aligned} \dot{M} &= M_{\text{BH}, 6}^{-0.5} \times M_*^2 \times R_*^{-1.5} \times \dot{M}_a(T_{\text{vis}}, \beta) \\ t_m &= (1+z) \times M_{\text{BH}, 6}^{0.5} \times M_*^{-1} \times R_*^{1.5} \times t_a(T_{\text{vis}}, \beta) \end{aligned} \quad (6)$$

, where $M_{\text{BH}, 6}$, M_* , R_* and z represent central BH mass in unit of $10^6 M_\odot$, stellar mass in unit of M_\odot , stellar radius in

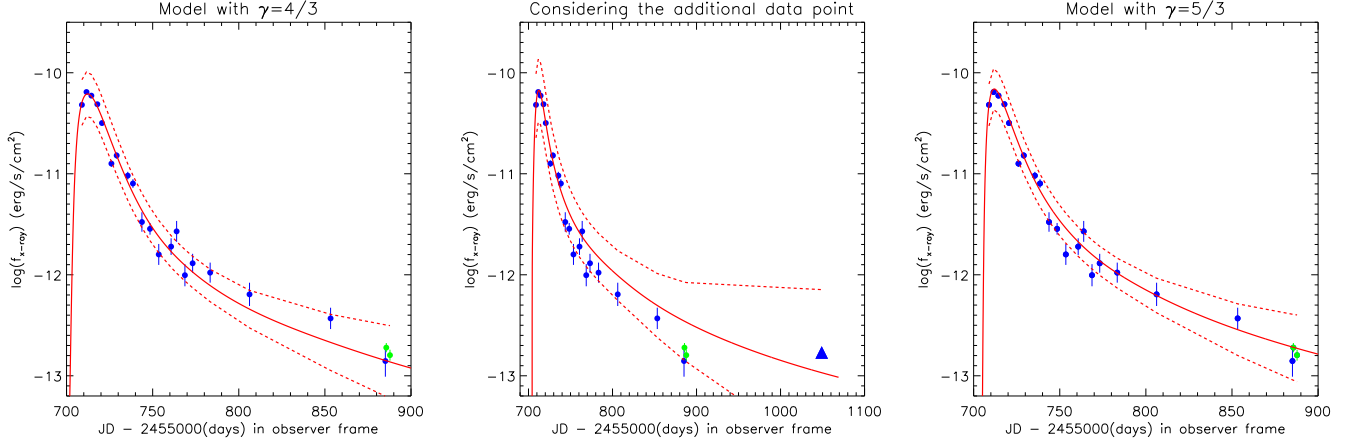


Figure 1. Left panel shows the X-ray light curve in the bandpass of 0.3-10keV of *Swift* J2058.4+0516 with JD from 2455708.915 to 2455887.787, and the best descriptions (shown in solid red line) and the corresponding 99% confidence bands (shown in dashed red lines) determined by the theoretical TDE model with $\gamma = 4/3$. Middle panel shows the light curve including the additional data point shown as solid blue triangle with JD=2456049.048, and the best descriptions (shown in solid red line) and the corresponding 99% confidence bands (shown in dashed red lines) determined by the theoretical TDE model with $\gamma = 4/3$. Right panel shows the light curve with JD from 2455708.915 to 2455887.787, and the best descriptions (shown in solid red line) and the corresponding 99% confidence bands (shown in dashed red lines) determined by the theoretical TDE model with $\gamma = 5/3$. In each panel, solid circles plus error bars in blue show the 20 data points acquired with the X-Ray Telescope on the Swift satellite, and solid circles plus error bars in green show the two data points acquired with the European Photon Imaging Camera on the XMM-Newton Observatory. In middle panel, the solid blue triangle plus error bars show the additional data point with JD=2456049.048 acquired with the European Photon Imaging Camera on the XMM-Newton Observatory.

unit of R_{\odot} and redshift of host galaxy of a TDE, respectively. And the mass-radius relation well discussed in [Tout \(1996\)](#) is accepted for main-sequence stars.

Fourth, based on the calculated time-dependent templates of accretion rate $\dot{M}(t)$, the modeled time-dependent bolometric luminosity $L_{\text{bol}, t}$ can be well determined. Meanwhile, accepted the strong correlation between X-ray luminosity and bolometric luminosity, the TDE model expected X-ray band flux $f_{\text{X-ray}, m}$ can be simply calculated as

$$\begin{aligned} L_{\text{bol}, t} &= \eta \times \dot{M}(t) \times c^2 \\ f_{\text{X-ray}, m} &= \frac{1}{k_{\text{bol}}} \times \frac{L_{\text{bol}, t}}{4 \pi D_{\text{obj}}^2} \end{aligned} \quad (7)$$

, where c , η , k_{bol} and D_{obj} represent the light speed, energy transfer efficiency around BH, the corresponding expected bolometric correction factor $k_{\text{bol}} = \frac{L_{\text{bol}}}{L_{\text{X-ray}}}$ (where L_{bol} and $L_{\text{X-ray}}$ as bolometric luminosity and X-ray band luminosity), and the distance of the *Swift* J2058.4+0516 which can be well estimated by the redshift, respectively.

Fifth, as results discussed on birth of relativistic jets related to TDEs ([Burrows et al. 2011](#); [Zauderer et al. 2011](#); [Berger et al. 2012](#)), a free model parameter Γ , the relativistic Lorentz factor, has been considered to correct the beaming effects in TDE model simulated time duration t and flux density f by

$$\begin{aligned} t_{\text{re}} &= t_m \times \Gamma \\ f_{\text{re}} &= f_m \times \Gamma^{n_{\gamma}} \end{aligned} \quad (8)$$

, where "t" and "f" mean the time information and corresponding X-ray band fluxes, subscripts of "m" and "re" represent values from the common theoretical TDE model and the values after considering the relativistic beaming effects, respectively. Here, n_{γ} is the well discussed parameter in [Cohen et al. \(2007\)](#). Moreover, as discussed results in [Cenko et al. \(2012\)](#) for *Swift* J2058.4+0516 and discussed results in [Burrows et al. \(2011\)](#) for the first relativistic TDE in *Swift* J1644+57 to make the birth of relativistic jets, the reasonable Γ could be larger than 2.1 and/or around 10-20.

Finally, the theoretical TDE model expected time dependent X-ray light curve can be described by the following eight model parameters, the central BH mass M_{BH} , the stellar mass M_{\star} (corresponding stellar radius R_{\star} tied by the mass-radius relation), the energy transfer efficiency η , the impact parameter β , the viscous timescale T_{vis} , the bolometric correction k_{bol} , the Lorentz factor Γ and the parameter n_{γ} . Meanwhile, the parameter of redshift of *Swift* J2058.4+0516 has been determined and accepted as $z = 1.1853$, through the spectroscopic features of Fe II and Mg I shown in [Cenko et al. \(2012\)](#).

3. MAIN RESULTS AND NECESSARY DISCUSSIONS

3.1. Fitting the X-ray light curve

The reported X-ray light curve in the bandpass of 0.3-10keV of *Swift* J2058.4+0516 in [Pasham et al. \(2015\)](#) is shown in left panel of Fig. 1 in observer frame. Similar long-term X-ray variabilities can also be found in the website of <https://tde.space> and in [Cenko et al. \(2012\)](#). It is clear that the

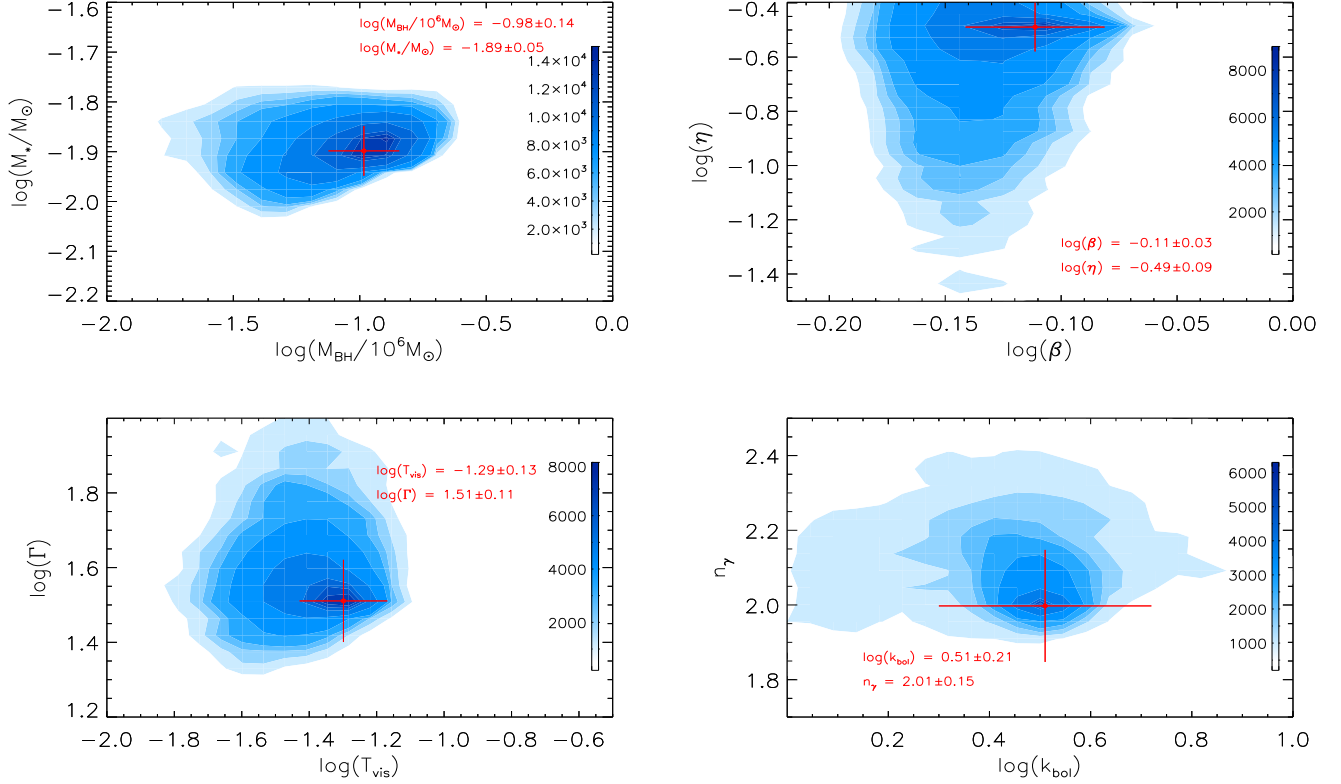


Figure 2. The MCMC determined two-dimensional projections of the posterior distributions in contour of the eight model parameters of $\log(M_{\text{BH}})$, $\log(M_\star)$, $\log(\beta)$, $\log(\eta)$, $\log(T_{\text{vis}})$, $\log(k_{\text{bol}})$, $\log(\Gamma)$ and n_γ through application of the theoretical TDE model with $\gamma = 4/3$. In each panel, solid circle plus error bars in red show the accepted values and uncertainties of the model parameters which are also marked by red characters in each panel.

smoothly declined trend was probably similar as TDE model expected time-dependent variabilities, as the results shown in Cenko et al. (2012): "the time-dependent X-ray variabilities can be described as $L_{X\text{-ray}} \propto t^{-2.2}$, with slope of -2.2 slightly different from the standard value of $-5/3$ ". As discussed in Guillochon & Ramirez-Ruiz (2013), only the extremely ideal cases for TDE with constant binding energy of the fallback materials to the BH $dM/dE = \text{constant}$ (M as debris mass and E the specific binding energy), the power law of accretion rates (luminosity) on time can be well expected by $t^{-5/3}$. However, for TDEs with dM/dE depending on E , the expected power law t^α could have α different from $-5/3$, such as the detailed discussions in Guillochon & Ramirez-Ruiz (2013), power law with $\alpha \sim -2.2$ steeper than standard $-5/3$ can be well accepted in TDEs.

There are 22 data points shown as solid circles in left panel of Fig. 1. Detailed descriptions on the 22 data points can be found in Pasham et al. (2015), simple descriptions on the 22 data points are described as follows. The 22 data points were acquired with two different instruments, 20 data points (shown as solid blue circles) with JD from 2455708.915 to 2455885.11 are from the X-Ray Telescope (Burrows et al. 2005) on the Swift satellite (Gehrels et al. 2004), and the

other two data points (shown as solid green circles) are from the European Photon Imaging Camera (Struder et al. 2001; Turner et al. 2001) on the XMM-Newton Observatory (Jansen et al. 2001). Moreover, there is one additional data point marked as solid blue triangle with JD=2456049.048 shown in middle panel of Fig. 1, which was acquired with the European Photon Imaging Camera on the XMM-Newton Observatory and will be discussed individually in the following paragraphs. Now, it is interesting to show that the theoretical TDE model can be applied to well describe the X-ray light curve of *Swift* J2058.4+0516 by the procedure described in Section 2.

Then, based on the theoretical TDE model described in Section 2, the observed X-ray light curve in the bandpass of 0.3-10keV of *Swift* J2058.4+0516 in observer frame shown in left panel of Fig. 1 can be well described by the TDE model with the tidally disrupted main-sequence star with polytropic index $\gamma = 4/3$, through the well-known maximum likelihood method combining with the Markov Chain Monte Carlo (MCMC) technique (Foreman-Mackey et al. 2013). And the corresponding 99% confidence bands are also shown in the left panel to the best descriptions to the X-ray light curve. When the theoretical TDE model is applied, there is only one

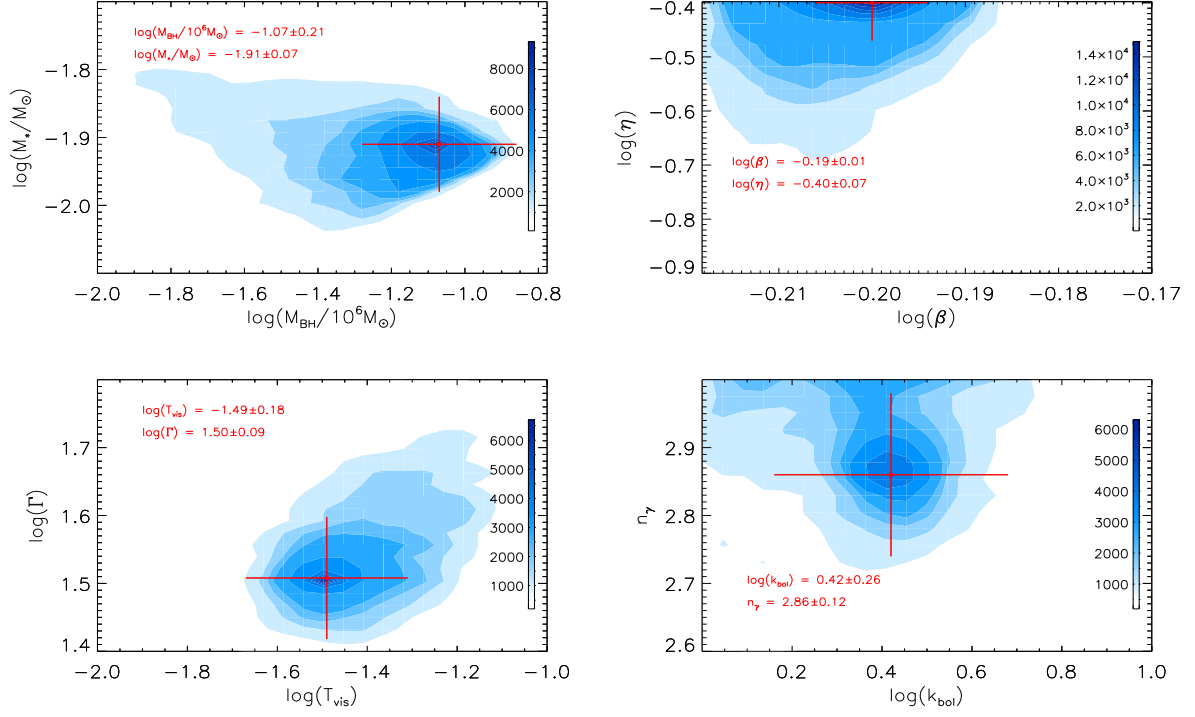


Figure 3. Similar as Fig. 2, but for the light curve including the additional data point with JD = 2456049.048 described by the theoretical TDE model with $\gamma = 4/3$ shown in middle panel of Fig. 1.

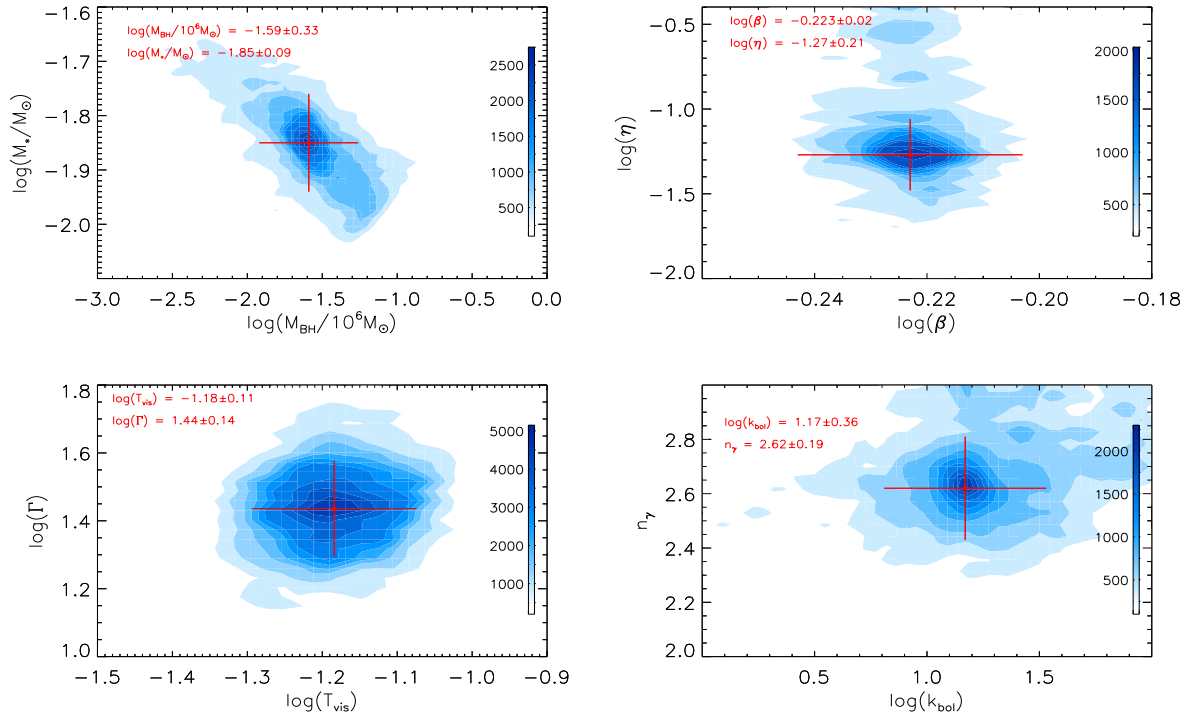


Figure 4. Similar as Fig. 2, but for the results shown in right panel of Fig. 1 through application of the theoretical TDE model with $\gamma = 5/3$.

criterion to limit the model parameters. For an available TDE with model parameters, the determined tidal disruption radius R_{TDE} ,

$$\frac{R_{\text{TDE}}}{R_s} = 5.06 \times (M_\star)^{-1/3} \left(\frac{M_{\text{BH}, 6}}{10}\right)^{-2/3} \times R_\star > 1 \quad (9)$$

, is larger than event horizon of central BH ($R_s = 2GM_{\text{BH}}/c^2$).

And the model parameters with accepted prior uniform distributions as follows, when the fitting procedure is running. The BH mass $\log(M_{\text{BH}}/10^6 M_\odot)$ has a prior uniform distribution from -3 to 3 and has 0 as the starting value. The stellar mass $\log(M_\star/M_\odot)$ has a prior uniform distribution from -2 to 1.78 (about $60M_\odot$) and has 0 as the starting value. The Lorentz factor $\log(\Gamma)$ has a prior uniform distribution from 0 to 1.7 and has 1 as the starting value. The impact parameter of $\log(\beta)$ has a prior uniform distribution from $\log(0.6)$ to $\log(4)$ for main sequence stars with polytropic index of 4/3 and has 0 as the starting value. The parameter of $\log(k_{\text{bol}})$ has a prior uniform distribution from $\log(2)$ to $\log(100)$ and has 2 as the starting value. The parameter of $\log(T_{\text{vis}})$ has a prior uniform distribution from -3 to 0 and has -1 as the starting value. The parameter of $\log(\eta)$ has a prior uniform distribution from $\log(0.005)$ to $\log(0.4)$ and has $\log(0.15)$ as the starting value. And the parameter of n_γ has a prior uniform distribution from 1 to 5 and has 2 as the starting value. Moreover, not similar as the different mass limits in [Guillochon & Ramirez-Ruiz \(2013\)](#); [Mockler et al. \(2019\)](#) for main-sequences stars with different polytropic indices, the same mass limits are accepted for main sequence stars with different polytropic indices by the following main consideration. [Guillochon & Ramirez-Ruiz \(2013\)](#); [Guillochon et al. \(2014\)](#); [Mockler et al. \(2019\)](#) have created the templates of dM/dE for the cases with $\gamma = 5/3$ after considerations of a main sequence star with stellar mass about one solar mass, indicating main sequence stars with $\gamma = 5/3$ but with masses larger than 0.3 solar masses and smaller than 22 solar masses could be theoretically accepted. Therefore, similar mass limits are accepted for main sequence stars with different polytropic indices in the manuscript.

The well MCMC determined posterior distributions of the model parameters are shown in Fig. 2, and accepted that $\log(M_{\text{BH}}/10^6 M_\odot) = -0.98 \pm 0.14$ ($M_{\text{BH}} \sim 1.05^{+0.39}_{-0.29} \times 10^5 M_\odot$), $\log(M_\star/M_\odot) = -1.89 \pm 0.05$, $\log(\beta) = -0.11 \pm 0.03$, $\log(\eta) = -0.49 \pm 0.09$, $\log(T_{\text{vis}}) = -1.29 \pm 0.13$, $\log(\Gamma) = 1.51 \pm 0.11$, $\log(k_{\text{bol}}) = 0.51 \pm 0.21$ and $n_\gamma = 2.01 \pm 0.15$. The information of the model parameters are also listed in Table 1. The large value of $\eta \sim 32\%$ can be well expected due to the relativistic jets in *Swift* J2058.4+0516. And the small value of $k_{\text{bol}} \sim 3.2$ is also can be acceptable value, as the shown results in [Lusso et al. \(2012\)](#) on ratios of bolometric luminosities to X-ray band luminosities of X-ray selected AGN. And the determined $\Gamma \sim 32$

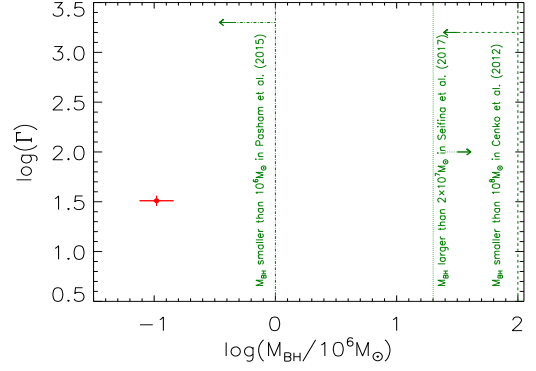


Figure 5. Properties of BH mass of *Swift* J2058.4+0516 determined by the theoretical TDE model and reported in the literature. Solid circle plus error bars in red show the results determined by the theoretical TDE model in the manuscript. The vertical dotted line in dark green shows the lower limit of central BH mass of *Swift* J2058.4+0516 discussed in [Seifina et al. \(2017\)](#): BH mass larger than $2 \times 10^7 M_\odot$. The vertical dashed line in dark green shows the upper limit of central BH mass of *Swift* J2058.4+0516 discussed in [Cenke et al. \(2012\)](#): BH mass smaller than $10^8 M_\odot$. The vertical dot-dashed line in dark green shows the upper limit of central BH mass of *Swift* J2058.4+0516 discussed in [Pasham et al. \(2015\)](#): BH mass between $10^4 M_\odot$ to $10^6 M_\odot$.

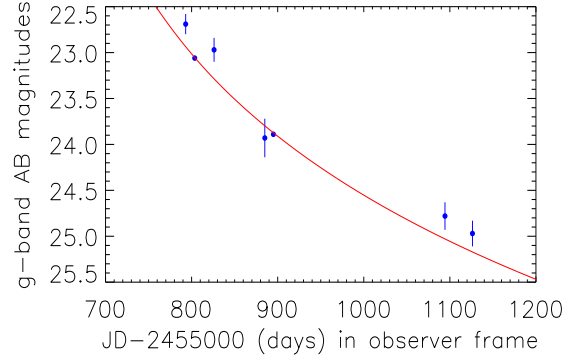


Figure 6. The g-band optical light curve (solid circles plus error bars in blue) of *Swift* J2058.4+0516 in observer frame, and the descriptions (solid red line) to the optical light curve by the shifted and weakened best descriptions to the X-ray light curve.

is a bit larger than the expected values around 10-20 in [Burrows et al. \(2011\)](#); [Cenke et al. \(2012\)](#), however, $\Gamma \sim 32$ is one common value as the discussed results in [Cohen et al. \(2007\)](#). And, the determined value of $n_\gamma \sim 2.01$ is well agreement with the expected global mean value as discussed in [Cohen et al. \(2007\)](#). All the determined model parameters have common values, and the BH mass is estimated as $M_{\text{BH}} \sim 1.05 \times 10^5 M_\odot$ in *Swift* J2058.4+0516 through the theoretical TDE model. The reported information of BH mass of *Swift* J2058.4+0516 are shown in Fig. 5, the determined

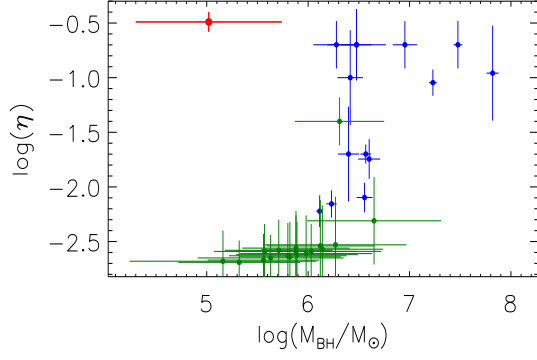


Figure 7. On the dependence of energy transfer efficiency η on central BH mass of the reported TDE candidates in Mockler et al. (2019); Zhou et al. (2021). Symbols in blue represent the results collected from Table 2 in Mockler et al. (2019), and symbols in dark green represent the results collected from Table 3 in Zhou et al. (2021). The solid circle plus error bars in red show the results for the *Swift* J2058.4+0516 determined in the manuscript.

BH mass $M_{BH} \sim 1.05 \times 10^5 M_\odot$ in *Swift* J2058.4+0516 is close to the previous results well discussed in Pasham et al. (2015) but far from the other reports on BH mass discussed in Cenko et al. (2012); Seifina et al. (2017).

Moreover, three points are noted, before giving further discussions on the best-fitting results and the determined model parameters by the theoretical TDE model.

First and foremost, the circularization processes in TDEs are not considered in *Swift* J2058.4+0516. More recent discussions on theoretical circularization processes can be found in Hayasaki et al. (2016); Zanazzi & Ogilvie (2020); Lynch & Ogilvie (2021). Observational circularization emissions in TDEs have been reported and discussed in the unique TDE candidate ASASSN-15lh in Leloudas et al. (2016), due to the two clear peaks detected in the UV band light curves. However, as the shown light curve in Fig. 1 of *Swift* J2058.4+0516, there are no re-brightened peaks. Certainly, Dong et al. (2016) have previously reported the ASASSN-15lh as a highly super-luminous supernova. If the ASASSN-15lh is not a TDE, the second UV peak in ASASSN-15lh is therefore not an unambiguous signature of delayed circularization. However, as commonly discussed in Mockler et al. (2019); Jiang et al. (2016); Lynch & Ogilvie (2021); Zhou et al. (2021), common circularization emissions can lengthen the rise-to-peak timescale in TDEs expected variabilities. The lengthened rise-to-peak timescale can lead to apparently large T_{vis} , when the theoretical TDE model is applied to describe the variabilities. However, the determined parameter $\log(T_{vis}) = -1.29 \pm 0.13$ can lead the expected viscous timescale T_{vis} in *Swift* J2058.4+0516 to be about 0.05 days , after considering the scaling factor $M_{BH,6}^{0.5} M_\star^{-1} R_\star^{1.5}$ shown in equation (6). The small value of 0.05 days strongly

indicates few effects of circularization emissions on our final results in *Swift* J2058.4+0516. Therefore, the simple case is mainly considered in *Swift* J2058.4+0516 that the fallback timescales of the circularization processes are significantly smaller than the viscous timescales of the accretion processes, and the fallback materials will circularize into a disk as soon as possible.

Besides, the light curve with data points shown as solid circles in left panel of Fig. 1 has time durations about 179days in observer frame, however, there is an additional data point with JD=2456049.048 and X-ray flux $0.17 \times 10^{-12} \text{ erg/s/cm}^2$ in Pasham et al. (2015) not included in the light curve. Middle panel of Fig. 1 shows the light curve including the additional data point shown as solid blue triangle. Based on the following two points, there are no further considerations and discussions on the additional data point with JD=2456049.048. On the one hand, the time dependent X-ray flux variabilities at late times should be roughly described by $t^{-5/3}$, however, the time dependent X-ray flux variabilities from JD=2455885 to JD=2456049 (time duration about 164days) are simply described by t^0 . On the other hand, if the additional data point with JD=2456049.048 is included in the light curve to be described by the theoretical TDE model, best-fitting results and corresponding 99% confidence bands shown in middle panel of Fig. 1 can also be determined based on the same prior distributions of the model parameters, however, the fitting results are worse for the data points with JD smaller than 2455887. And the posterior distributions of the model parameters are shown in Fig. 3 with determined central BH mass about $\log(M_{BH}/10^6 M_\odot) \sim -1.07 \pm 0.21$, which is similar as the determined BH mass $\log(M_{BH}/10^6 M_\odot) = -0.98 \pm 0.14$ without consideration of the additional data point with JD=2456049.048. Here, there are no further discussions on the model parameters shown in Fig. 3 and listed in Table 1. The main objective to show the posterior distributions of the model parameters is to assure acceptable model parameters through the theoretical TDE model applied to describe the X-ray light curve including the additional data point with JD=2456049.048. Therefore, the additional data point with JD=2456049.048 is not considered and discussed any more in the manuscript.

Last but not the least, besides the best fitting results to the long-term X-ray variabilities in left panel of Fig. 1 determined by the theoretical TDE model with the polytropic index $\gamma = 4/3$, similar best fitting results to the X-ray light curve can also be determined by application of theoretical TDE model with the polytropic index $\gamma = 5/3$. The same prior uniform distributions and starting values are accepted to the model parameters, besides a prior uniform distribution of the impact parameter of $\log(\beta)$ from $\log(0.50)$ to $\log(2.5)$ for main sequence stars with polytropic index of $\gamma = 5/3$. The determined best fitting results and correspond-

Table 1. Basic information of the model parameters applied to fit X-ray light curve of *Swift* J2058.4+0516

	$\log(M_{BH}/10^6 M_\odot)$	$\log(M_*/M_\odot)$	$\log(\beta)$	$\log(\eta)$	$\log(T_{vis})$	$\log(\Gamma)$	$\log(k_{bol})$	n_γ
theoretical TDE model with $\gamma = 4/3$ applied to describe the light curve shown in left panel of Fig. 1								
limits	[-3, 3]	[-2, 1.78]	[-0.22, 0.6]	[-2.3, -0.4]	[-3, 0]	[0, 1.7]	[0.30, 2]	[1, 5]
P_0	0	0	0	-0.8	-1	1	1	2
P_M	-0.98 ± 0.14	-1.89 ± 0.05	-0.11 ± 0.03	-0.49 ± 0.09	-1.29 ± 0.13	1.51 ± 0.11	0.51 ± 0.21	2.01 ± 0.15
theoretical TDE model with $\gamma = 4/3$ applied to describe the light curve shown in middle panel of Fig. 1								
limits	[-3, 3]	[-2, 1.78]	[-0.22, 0.6]	[-2.3, -0.4]	[-3, 0]	[0, 1.7]	[0.30, 2]	[1, 5]
P_0	0	0	0	-0.8	-1	1	1	2
P_M	-1.07 ± 0.21	-1.91 ± 0.07	-0.19 ± 0.01	-0.40 ± 0.07	-1.49 ± 0.18	1.50 ± 0.09	0.42 ± 0.26	2.86 ± 0.12
theoretical TDE model with $\gamma = 5/3$ applied to describe the light curve shown in right panel of Fig. 1								
limits	[-3, 3]	[-2, 1.78]	[-0.3, 0.4]	[-2.3, -0.4]	[-3, 0]	[0, 1.7]	[0.30, 2]	[1, 5]
P_0	0	0	0	-0.8	-1	1	1	2
P_M	-1.59 ± 0.33	-1.85 ± 0.09	-0.223 ± 0.02	-1.27 ± 0.21	-1.18 ± 0.11	1.44 ± 0.14	1.17 ± 0.36	2.62 ± 0.19

Notice: There are nine columns in the table. The second to the last columns show the information of the eight model parameters in the theoretical TDE model discussed in Section 2. The row with the first column named "limits" shows the information of the accepted limits of the prior uniform distributions of the model parameters. The row with the first column named " P_0 " shows the starting values of the model parameters, when the procedure is running to fit the X-ray light curve. The row with the first column named " P_M " shows the determined values of the model parameters through the MCMC determined posterior distributions.

The third to the fifth rows show the basic information of the model parameters in the theoretical TDE model with $\gamma = 4/3$ applied to describe the light curve shown in left panel of Fig. 1, with the corresponding MCMC determined posterior distributions of the model parameters shown in Fig. 2.

The seventh to the ninth rows show the basic information of the model parameters in the theoretical TDE model with $\gamma = 4/3$ applied to describe the light curve including the additional data point with JD=2456049.048 shown in middle panel of Fig. 1, with the corresponding MCMC determined posterior distributions of the model parameters shown in Fig. 3.

The eleventh to the thirteenth rows show the basic information of the model parameters in the theoretical TDE model with $\gamma = 5/3$ applied to describe the light curve shown in right panel of Fig. 1, with the corresponding MCMC determined posterior distributions of the model parameters shown in Fig. 4.

ing 99% confidence bands are shown in right panel of Fig. 1 to the X-ray light curve, and the posterior distributions of the model parameters are shown in Fig. 4 and the accepted values listed in Table 1. The determined central BH mass is about $\log(M_{BH}/10^6 M_\odot) \sim -1.59 \pm 0.33$, a bit smaller BH mass determined by the model with $\gamma = 4/3$. However, considering the following main reason, the results determined by the model with $\gamma = 5/3$ are not preferred. The determined energy transfer efficiency η is about $\eta \sim 0.054^{+0.033}_{-0.021}$, indicating a central non-spinning Schwarzschild BH, not reasonable to explain the relativistic jet in *Swift* J2058.4+0516. Therefore, in the manuscript, rather than the TDE model with $\gamma = 5/3$, the theoretical TDE model with $\gamma = 4/3$ is preferred to determine the final best descriptions to the long-term X-ray variabilities in *Swift* J2058.4+0516.

3.2. Further discussions

First and foremost, based on the reported results in [Cenko et al. \(2012\)](#) and in [Seifina et al. \(2017\)](#), previously expected BH mass could be larger than $2 \times 10^7 M_\odot$ and smaller than $10^8 M_\odot$. Here, we can check whether so large BH mass could be reasonable in *Swift* J2058.4+0516. Unfortunately,

once accepted the prior uniform distribution of BH mass $\log(M_{BH}/10^6 M_\odot)$ from $\log(20)$ to $\log(100)$, the observed X-ray light curve of *Swift* J2058.4+0516 can not be described by the model parameters within the accepted prior distributions. Therefore, the central BH mass of *Swift* J2058.4+0516 is preferred to be about $1.05^{+0.39}_{-0.29} \times 10^5 M_\odot$, through the theoretical TDE model. The determined BH mass well consistent with the results discussed in [Pasham et al. \(2015\)](#).

Besides, we do not consider properties of the previously reported steep drop (or turnoff) in the X-ray variabilities at late times in *Swift* J2058.4+0516, such as discussed results in [Pasham et al. \(2015\)](#), which would be related to the transition from super-Eddington to sub-Eddington accretion as discussed in [Pasham et al. \(2015\)](#) or to accretion disk transitioned from a thick disk to a thin disk as suggested in [Mangano et al. \(2016\)](#) for the *Swift* J1644+57. Therefore, the proposed TDE model above cannot be applied to explain or to anticipate the steep drop at late times in *Swift* J2058.4+0516, but the collected long-term X-ray variabilities not including the steep drop features can provide sufficient information to determine the central BH mass by the theoretical TDE model.

Last but not the least, it is a better idea to apply the same TDE model parameters to describe the long-term optical light curve of *Swift* J2058.4+0516, in order to confirm the reliability of the determined TDE model parameters, especially the central BH mass. Fortunately, there are 7 reliable data points in each optical *ugriz* bands in Pasham et al. (2015). Then, we check whether the TDE model expected best descriptions to the X-ray light curve can be applied to describe the optical light curve. Here, the g-band light curve in observer frame is collected from Table 2 in Pasham et al. (2015) and shown in Fig. 6. However, there are quite few data points in the optical g-band light curve of *Swift* J2058.4+0516, and there is not clear peak information of the optical light curve, not similar as the X-ray light curve of *Swift* J2058.4+0516. Therefore, not the detailed MOSFIT code or the TDEFIT code is applied to described the optical light curve of *Swift* J2058.4+0516, but the TDE model determined best descriptions to the X-ray light curve weakened by a factor about 1430 and shifted by -117days can be well applied to describe the optical light curve of *Swift* J2058.4+0516. The weakened factor of 1430 could be a reasonable value, such as the ratios round 1000 of X-ray luminosities to optical luminosities of *Swift* J2058.4+0516 shown in Figure 1 in Pasham et al. (2015). And the descriptions to the optical g-band light curve is shown in Fig. 6, indicating that the similar TDE model can be also applied to describe optical variabilities, indicating the determined TDE model parameters are reliable enough.

Before the end of the section, further discussions are given on the determined central BH mass of *Swift* J2058.4+0516. Among the reported central BH masses of TDE candidates in Guillochon et al. (2014); Mockler et al. (2019), the *Swift* J2058.4+0516 has the smallest central BH mass. Even considering the more recent reported BH masses of TDE candidates in Zhou et al. (2021) which are systematically smaller than the BH masses estimated in Mockler et al. (2019), the *Swift* J2058.4+0516 also has the smallest central BH mass, accepted mean BH mass $1.15 \times 10^5 M_\odot$ in iPTF16fnl in Zhou et al. (2021). Meanwhile, among the reported energy transfer efficiencies η of TDE candidates in Guillochon et al. (2014); Mockler et al. (2019); Zhou et al. (2021), the *Swift* J2058.4+0516 has the largest energy transfer efficiency η . Fig. 7 shows the dependence of energy transfer efficiency η on central BH mass of the reported TDE candidates in Mockler et al. (2019); Zhou et al. (2021). Here, only the main values of iPTF16fnl and GALEX D23H-1 are collected from the Table 3 in Zhou et al. (2021). The results shown in Fig. 7 strongly indicate that the *Swift* J2058.4+0516 is one unique TDE candidate among the reported TDE candidates. Furthermore, the inconsistent dependence of energy transfer efficiency on central BH mass between the *Swift* J2058.4+0516 and the other TDE candidates provides fur-

ther clues to detect and/or anticipate candidates of relativistic TDE to make the birth of relativistic jets.

4. MAIN SUMMARIES AND CONCLUSIONS

Finally, our main summaries and conclusions are as follows.

- Long-term X-ray variabilities of *Swift* J2058.4+0516 with JD from 2455708.915 to 2455887.787 can be well described by a main-sequence star with $\gamma = 4/3$ tidally disrupted by a central BH with mass about $\log(M_{BH}/10^6 M_\odot) = -0.98 \pm 0.14$ and with energy transfer efficiency about 32%, to support a central rapid spinning low mass BH in *Swift* J2058.4+0516.
- Long-term X-ray variabilities of *Swift* J2058.4+0516 with JD from 2455708.915 to 2455887.787 can also be well described by a main-sequence star with $\gamma = 5/3$ tidally disrupted by a central BH with energy transfer efficiency about 5%, indicating a central non-spinning low mass BH. Considering the relativistic jet in *Swift* J2058.4+0516, the determined model parameters with $\gamma = 5/3$ are not preferred.
- Considering the additional data point with JD=2456049.048, there are similar central BH masses in *Swift* J2058.4+0516 determined by applications of theoretical TDE model to describe the X-ray light curve including the additional data point.
- Based on the long-term X-ray variability properties well described by the theoretical TDE model in *Swift* J2058.4+0516, the central BH mass can be well determined as $1.05^{+0.39}_{-0.29} \times 10^5 M_\odot$, after well considering the relativistic beaming effects.
- Based on the reported BH mass and energy transfer efficiency of TDE candidates, the *Swift* J2058.4+0516 is an unique TDE candidate in the space of BH mass versus energy transfer efficiency, providing further clues to detect and/or anticipate candidates of relativistic TDEs to make the birth of relativistic jets.

ACKNOWLEDGEMENTS

Zhang gratefully acknowledges the anonymous referee for giving us constructive comments and suggestions to greatly improve our paper. Zhang gratefully acknowledges the kind support of Starting Research Fund of Nanjing Normal University and the kind financial support from NSFC-12173020. The paper has made use of the public code of TDEFIT (<https://github.com/guillochon/tdefit>) and MOSFIT (<https://github.com/guillochon/mosfit>).

REFERENCES

- Anderson, M., Mooley, K., Hallinan, G., et al., 2020, *ApJ*, 903, 116
- Barthelmy, S. D.; Barbier, L. M.; Cummings, J. R.; et al., 2005, *Space Science Reviews*, 120, 143
- Berger, E.; Zauderer, A.; Pooley, G. G.; et al., 2012, *ApJ*, 748, 36
- Burrows, D. N.; Hill, J. E.; Nousek, J. A.; et al. 2005, *Space Science Reviews*, 120, 165
- Burrows, D. N.; Kennea, J. A.; Ghisellini, G.; et al., 2011, *Natur*, 476, 421
- Cenko, S. B.; Krimm, H. A.; Horesh, A.; et al., 2012, *ApJ*, 735, 77
- Cohen, M. H., Lister, M. L., Homan, D. C.; et al., 2007, *ApJ*, 658, 232
- Dong, S.; Shappee, B. J.; Prieto, J. L.; et al., 2016, *Science*, 351, 257
- Gezari, S., et al., 2012, *Nature*, 485, 217
- Eftekhari, T.; Berger, E.; Zauderer, B. A.; Margutti, R.; K. D. Alexander I, K. D., 2018, *ApJ*, 854, 86
- Ferrarese, F. & Merritt, D., 2000, *ApJL*, 539, 9
- Gebhardt, K., et al., 2000, *ApJL*, 539, 13
- Gehrels, N.; Chincarini, G. ; Giommi, P.; et al., 2004, *ApJ*, 611, 1005
- Foreman-Mackey, D.; Hogg, D. W.; Lang, D.; Goodman, J., 2016, *PASP*, 125, 306
- Gromadzki, M.; Hamanowicz, A.; Wyrzykowski, L.; et al., 2019, *A&A*, 622, 2
- Guillochon, J. & Ramirez-Ruiz, E., 2013, *ApJ*, 767, 25
- Guillochon, J.; Manukian, H.; Ramirez-Ruiz, E., 2014, *ApJ*, 783, 23
- Guillochon, J.; Nicholl, M.; Villar, A., et al., 2018, *ApJS*, 236, 6
- Gultekin, K., Cackett, E. M., Miller, J. M.; et al., 2009, *ApJ*, 706, 404
- Kimitake Hayasaki, K.; Stone, N.; Loeb, A., 2016, *MNRAS*, 461, 3760
- Hinkle, J. T., et al., 2021, *MNRAS*, 500, 1673
- Holoien, T. W. S., et al., 2016, *MNRAS*, 455, 2918
- Jansen, F., Lumb, D., Altieri, B., et al. 2001, *A&A*, 365, L1
- Jiang, Y. F.; Guillochon, J.; Loeb, A. 2016, *ApJ*, 830, 125
- Komossa, S.; Bade, N., 1999, *A&A*, 343, 775
- Komossa, S.; Halpern, J.; Schartel, N., et al., 2004, *ApJL*, 603, 17
- Kormendy, J. & Ho, L. C., 2013, *ARA&A*, 51, 511
- Krolik, J. H.; Piran, T., 2011, *ApJ*, 743, 134
- Leloudas, G.; Fraser, M.; Stone, N. C., et al., 2016, *Natur Astronomy*, 1, 2
- Liu, F. K.; Zhou, Z. Q.; Cao, R.; Ho, L. C.; Komossa, S., 2017, *MNRAS Letter*, 472, 99
- Lusso, E.; Comastri, A.; Simmons, B. D.; et al., 2012, *MNRAS*, 425, 623
- Lynch, E. M., Ogilvie, G. I., 2021, *MNRAS*, 501, 5500
- Mangano, V.; Burrows, D. N.; Sbarufatti, B.; Cannizzo, J. K., 2016, *ApJ*, 817, 103
- Merloni, A., et al., 2015, *MNRAS*, 452, 69
- Mockler, B.; Guillochon, J.; Ramirez-Ruiz, E., 2019, *ApJ*, 872, 151
- Metzger, B. D., Stone, N. C. 2016, *MNRAS*, 461, 948
- Narayan, R.; McClintock, J. E.; Tchekhovskoy, A., 2014, *General Relativity, Cosmology and Astrophysics, Fundamental Theories of Physics*, 177, 523
- Peterson, B. M., et al., 2004, *ApJ*, 613, 682
- Rafiee, A. & Hall, P. B., 2011, *ApJS*, 194, 42
- Pasham, D. R.; Cenko, S. B.; Levan, A. J.; et al., 2015, *ApJ*, 805, 68
- Savorgnan, G. A. D. & Graham, A. W., 2015, *MNRAS*, 446, 2330
- Seifina, E.; Titarchuk, L.; Virgili, E., 2017, *A&A*, 607, 38
- Shaposhnikov, N. & Titarchuk, L., 2009, *ApJ*, 699, 453
- Shen, Y.; Richards, G. T.; Strauss, M. A.; et al., 2010, *ApJS*, 194, 45
- Struder, L.; Briel, U.; Dennerl, K.; et al. 2001, *A&A*, 365, L18
- Titarchuk, L., & Seifina, E., 2017, *A&A*, 602, 113
- Tout, C. A.; Pols, O.; Eggleton, P.; Han, Z., 1996, *MNRAS*, 281, 257
- Turner, M. J. L.; Abbey, A.; Arnaud, M.; et al. 2001, *A&A*, 365, L27
- van Velzen S., et al., 2011, *ApJ*, 741, 73
- van Velzen S., Gezari S., et al., 2019, *ApJ*, 872, 198
- Wang, T.; Yan, L.; Dou, L., et al., 2018, *MNRAS*, 477, 2943
- Wevers, T.; Nicholas C. Stone, N. C.; van Velzen, S.; et al., 2019, *MNRAS*, 487, 4816
- Wiersema, K.; Higgins, A. B.; Levan, A. J., et al., 2020, *MNRAS*, 491, 1771
- Wyrzykowski, L.; Zielinski, M.; Kostrzewa-Rutkowska, Z.; et al., 2017, *MNRAS Letter*, 465, L114
- Zanazzi, J. J.; Ogilvie, G. I., 2020, *MNRAS*, 499, 5562
- Zauderer, B. A.; Berger, E.; Soderberg, A. M.; et al., 2011, *Natur*, 476, 425
- Zhou, Z. Q.; Liu, F. K.; Komossa, S., et al., 2021, *ApJ*, 907, 77